



Integrated Genomic Profiling and Drug Screening of Patient-Derived Cultures Identifies Individualized Copy Number-Dependent Susceptibilities Involving PI3K Pathway and 17q Genes in Neuroblastoma

OPEN ACCESS

Edited by:

Kiyohiro Ando,
Saitama Cancer Center, Japan

Reviewed by:

Hongjuan Cui,
Southwest University, China
Ryuichi Sugino,
Saitama Cancer Center, Japan

*Correspondence:

Amos H. P. Loh
amos.loh.h.p@singhealth.com.sg

Specialty section:

This article was submitted to
Pediatric Oncology,
a section of the journal
Frontiers in Oncology

Received: 14 May 2021

Accepted: 28 September 2021

Published: 14 October 2021

Citation:

Wong RLY, Wong MRE,
Kuick CH, Saffari SE,
Wong MK, Tan SH, Merchant K,
Chang KTE, Thangavelu M,
Periyasamy G, Chen ZX, Iyer P,
Tan EEK, Soh SY, Iyer NG, Fan Q
and Loh AHP (2021) Integrated
Genomic Profiling and Drug
Screening of Patient-Derived
Cultures Identifies Individualized
Copy Number-Dependent
Susceptibilities Involving PI3K
Pathway and 17q Genes
in Neuroblastoma.
Front. Oncol. 11:709525.
doi: 10.3389/fonc.2021.709525

Rachel L. Y. Wong¹, Megan R. E. Wong², Chik Hong Kuick³, Seyed Ehsan Saffari⁴,
Meng Kang Wong², Sheng Hui Tan², Khurshid Merchant^{1,2,3}, Kenneth T. E. Chang^{1,2,3},
Matan Thangavelu⁵, Giridharan Periyasamy⁵, Zhi Xiong Chen^{2,6}, Prasad Iyer^{1,2,7},
Enrica E. K. Tan^{1,2,7}, Shui Yen Soh^{1,2,7}, N. Gopalakrishna Iyer^{1,8}, Qiao Fan⁴
and Amos H. P. Loh^{1,2,9*}

¹ Duke NUS Medical School, Singapore, Singapore, ² VIVA-KKH Paediatric Brain and Solid Tumour Programme, Children's Blood and Cancer Centre, KK Women's and Children's Hospital, Singapore, Singapore, ³ Department of Pathology and Laboratory Medicine, KK Women's and Children's Hospital, Singapore, Singapore, ⁴ Centre for Quantitative Medicine, Duke NUS Medical School, Singapore, Singapore, ⁵ Centre for High Throughput Phenomics (CHIP-GIS), Genome Institute of Singapore, Singapore, Singapore, ⁶ Department of Physiology, National University of Singapore, Singapore, Singapore, ⁷ Department of Paediatric Subspecialties Haematology Oncology Service, KK Women's and Children's Hospital, Singapore, Singapore, ⁸ Division of Medical Sciences, National Cancer Centre, Singapore, Singapore, ⁹ Department of Paediatric Surgery, KK Women's and Children's Hospital, Singapore, Singapore

Neuroblastoma is the commonest extracranial pediatric malignancy. With few recurrent single nucleotide variations (SNVs), mutation-based precision oncology approaches have limited utility, but its frequent and heterogenous copy number variations (CNVs) could represent genomic dependencies that may be exploited for personalized therapy. Patient-derived cell culture (PDC) models can facilitate rapid testing of multiple agents to determine such individualized drug-responses. Thus, to study the relationship between individual genomic aberrations and therapeutic susceptibilities, we integrated comprehensive genomic profiling of neuroblastoma tumors with drug screening of corresponding PDCs against 418 targeted inhibitors. We quantified the strength of association between copy number and cytotoxicity, and validated significantly correlated gene-drug pairs in public data and using machine learning models. Somatic mutations were infrequent (3.1 per case), but copy number losses in 1p (31%) and 11q (38%), and gains in 17q (69%) were prevalent. Critically, *in-vitro* cytotoxicity significantly correlated only with CNVs, but not SNVs. Among 1278 significantly correlated gene-drug pairs, copy number of GNA13 and DNA damage response genes CBL, DNMT3A, and PPM1D were most significantly correlated with cytotoxicity; the drugs most commonly

associated with these genes were PI3K/mTOR inhibitor PIK-75, and CDK inhibitors P276-00, SNS-032, AT7519, flavopiridol and dinaciclib. Predictive Markov random field models constructed from CNVs alone recapitulated the true z-score-weighted associations, with the strongest gene-drug functional interactions in subnetworks involving PI3K and JAK-STAT pathways. Together, our data defined individualized dose-dependent relationships between copy number gains of PI3K and STAT family genes particularly on 17q and susceptibility to PI3K and cell cycle agents in neuroblastoma. Integration of genomic profiling and drug screening of patient-derived models of neuroblastoma can quantitatively define copy number-dependent sensitivities to targeted inhibitors, which can guide personalized therapy for such mutationally quiet cancers.

Keywords: neuroblastoma, patient-derived culture, copy number variations (CNV), Comprehensive genomic profiling (CGP), PI3K - AKT pathway, CDK (cyclin-dependent kinase), JAK-STAT cascade

INTRODUCTION

Neuroblastoma is the most common pediatric extracranial malignant tumor and is responsible for a disproportionate 15% of all childhood cancer deaths. Despite current intensive multimodal therapy for patients with high-risk disease, 5-year survival remains at 30-50% even after decades of international multicenter trials. Due to its histologic and biologic heterogeneity, the classic stage- and risk-based clinical trial approach cannot adequately match treatments to the diverse individual susceptibilities of each patient's tumor, and is further limited by the small numbers of patients in each subgroup (1). Thus, therapeutic advancements for neuroblastoma may be better realized with a personalized approach.

Precision oncology approaches based on identification of targetable single nucleotide variants (SNVs) have limited usefulness in embryonal tumors because of their low mutational burden (2). Instead, copy number variations (CNVs) are more prevalent and are stronger prognostic factors in neuroblastoma (2–4). In particular, segmental chromosomal aberrations (SCAs) are associated with advanced disease stage and poorer prognosis. This corroborates with recent evidence that the pathogenicity of CNVs correlate with dosage sensitivity of involved genes, and are enriched for embryonal neurodevelopmental functions (5). This suggests that gene copy number could be used to predict and select targeted therapies, especially in embryonal tumors of childhood (6). While current sequencing-based panels may be an efficient and cost-effective manner to perform clinical genomic profiling, most are designed for adult cancers or hematological malignancies. Recently, the OncoPrint Childhood Cancer Research Assay (OCCRA) was developed as a diagnostic-grade genomic profiling tool curated specifically for pediatric cancers (7, 8). This is a promising new resource to detect significant and potentially actionable SNVs and CNVs in neuroblastoma.

Abbreviations: SNV, single nucleotide variant; CNV, copy number variation; SCA, segmental chromosomal aberration; OCCRA, OncoPrint Childhood Cancer Research Assay; PDC, patient-derived cell culture; FDR, false discovery rate; PGM, Probabilistic Graphical Model; CDK, cyclin dependent kinase.

Individualized preclinical tumor models can be a complementary means to rapidly test drug therapies *ex vivo*, and have been able to successfully uncover potential therapeutic leads (9, 10). While this has been employed extensively in epithelial carcinomas, embryonal tumors like neuroblastoma have not been consistently engrafted as personalized *in vitro* models. Commercial cell lines are often significantly changed with multiple serial passages or have been contaminated over time, and do not capture individual patient genetic or phenotypic differences in treatment response (11–14). We previously developed multi-lineage patient-derived cell cultures (PDCs) of neuroblastoma from pre- and post-treatment tumors and demonstrated their recapitulation of original tumors' chromosomal alterations, immunohistochemical and gene expression profiles, and ability to predict individualized responses to standard-of-care chemotherapy (15). However, the utility of patient-derived models for prediction of targeted therapies for neuroblastoma have not been well studied.

We hypothesize that in neuroblastoma, gene copy number and *in vitro* cytotoxicity to corresponding targeted inhibitors display distinct relationships in a dose-dependent manner. To study key genotype-phenotype correlations in neuroblastoma, we characterized SNVs and CNVs of neuroblastoma tumors using clinical genomic profiling and interrogated corresponding PDCs with a medium-throughput inhibitor screen, then correlated resulting genomic and phenotypic readouts. We then defined the quantitative associations between these genomic aberrations and the corresponding responses to targeted agents as a framework to potentially guide personalized targeted therapeutic options, particularly for patients with few or no targetable mutations.

MATERIALS AND METHODS

Patients and Tumor Samples

Patients with neuroblastoma were prospectively recruited at KK Women's and Children's Hospital with Institutional Review Board approval (CIRB 2014/2079). Written consent from parents, and assent from children were obtained. Criteria for

study inclusion were: patients under undergoing surgical biopsies or resections, with available excess tumor tissue; male and female patients with neuroblastoma aged 1–8 were included. No subject attrition was encountered, no randomization or power calculation was required, and investigators were blinded to patient identities. Excess tumor tissue from routine surgical procedures were transported on ice on the same day to the VIVA-KKH Paediatric Solid Tumour Laboratory for generation of PDCs. Corresponding tumor aliquots were snap frozen for molecular analysis.

OCCRA Comprehensive Genomic Profiling

Access to OCCRA (RRID : SCR_007834) (Thermo Fisher Scientific, Waltham, MA) was granted *via* an early access program. The DNA assay was utilized, which calls SNVs from hotspots of 86 genes and full exons of 44 genes, and CNVs from 28 genes. DNA was extracted from macro-dissected tissue using ReliaPrep FFPE DNA extraction kit (Promega, Madison, WI, USA). OCCRA primers and AmpliSeq Library Kit Plus (Illumina, San Diego, California, USA) were used for library preparation. The prepared libraries were sequenced using a MiniSeq sequencer (Illumina). Base calling and mapping to a reference genome (hg19) was performed using the BaseSpace Informatics suite (Illumina). SNV variant calling was performed with the DNA amplicon application (Illumina, version 2.1.1) and CNV calling was performed with the OncoCNV caller application (Illumina, version 1.2.0). All VCF files were loaded into variant interpreter (version 2.7.0.412) for interpretation. Criteria for selecting somatic SNV candidates were: >100 minimum coverage reads, 10% minimum allele frequency, cosmic reported variant, and <1% prevalence in the 1000 Genome Population Database.

Cell Culture

PDCs were generated as previously described by explant culture under growth conditions of 37°C with 5% CO₂ (15), and passaged at 1:2 split ratio upon reaching 80–100% confluence (15). For each PDC line, optimal seeding density to achieve 72-hour log-phase growth was determined. Cells of each PDC line were seeded on clear bottom white 96-well plates in triplicate (Corning, Cat 3903) in a 1:2 split ratio and assessed for appropriate responses to positive and negative control agents 0.5% DMSO and 1μM Staurosporine over 72-hours using IncuCyte[®] S3 Live-Cell Analysis System (RRID : SCR_019874) (Essen BioScience, Sartorius, Japan) and IncuCyte Base Software (v.2018B), using default analysis settings.

Short Tandem Repeat Fingerprinting

STR genotyping of all tumor-PDC pairs was performed using PowerPlex[®] 21 (Promega, Cat DC8902) using 1ng DNA. PCR products were resolved in an Applied Biosystems[®] SeqStudio genetic analyzer and compared.

Medium-Throughput Screening Assay

Selleckchem Kinase Inhibitor Library (SelleckChem, Cat. L1200), consisting of 418 tyrosine kinase inhibitors, was reformatted into 96-well format and diluted with DMSO to achieve final

concentrations of 1μM. Daughter plates were stored at -20°C and underwent no more than 15 freeze-thaw cycles.

Cells were seeded in a 1:2 dilution factor on 96-well white bottom plates (Corning, Cat 3917) using MultiFlo[™] FX (RRID : SCR_019746) (Biotek, Winooski VT). Plates were incubated for 24 hours at 37°C with 5% CO₂, and 0.5μL of each drug was added to the corresponding wells using Bravo BenchCel Workstation (RRID : SCR_019468) (Agilent, Santa Clara CA) equipped with automated liquid and microplate handling. Treated plates were centrifuged for 1 minute at 1000rpm before and incubated for the next 72 hours. Cytotoxicity was determined using CellTiter-Glo[®] Luminescent Cell Viability Assay (Promega, Cat G7572). Media was aspirated before adding 50μL of CellTiter-Glo reagent prepared as per manufacturer's protocol. Plates were shielded from light and agitated at 300rpm for 15 minutes; bioluminescence was measured using Infinite M1000 series microplate reader (Tecan, Mannerdorf, Switzerland) using a luminescence integration time of 250ms. Relative light units (RLUs) were normalized against DMSO negative controls of each corresponding plate to obtain normalized cytotoxicity values. Screening runs were validated only if high cytotoxicity to positive control staurosporine (1μM) and minimal DMSO effect were observed

Data Analysis

Clustering of copy number and z-score data was performed on ComplexHeatmap (v.2.0.0, RRID : SCR_017270) using R 3.6.1 with complete Euclidean clustering applied.

Pearson's correlation coefficients were calculated for each of 56,848 gene-drug pairs, comparing cytotoxicity and SNV, and cytotoxicity and copy number, using Fisher's z-transformation approach. Positive or negative drug-gene correlations were obtained for all 56,848 gene-drug combinations for both mutational variants and gene copy number. False discovery rates (FDR) for the Benjamini-Hochberg procedure were set at 0.1 as a threshold of statistical significance of gene-drug pairs (16). Data analysis was performed using R 4.0.3.

Probabilistic *In Silico* Model

Probabilistic Graphical Models (PGMs) were constructed with ReactomeFIViz (v. 7.2.3) using Reactome Functional Interaction (FI) network version 2018, which utilizes an adaptation of the PARADIGM approach (17–19) (RRID : SCR_009634). Briefly, this infers case-specific genetic variations, incorporating information from curated Reactome pathways, converting these reactions into factors then modeling the variations in each gene as constraint graphs which represent them as probability distribution functions. CNVs were input as continuous observation variables without discretizing and pairwise Markov random field models using empirical distributions were constructed over 100 permutations. Genes with mean differences in protein impact scores of <-0.01 and >0.01 between real and random samples were selected; genes with no CNV were removed. The PGM network was overlaid with associated Cancer Targetome drugs (20). A corresponding network was constructed from gene-drug pairs weighted according to z-scores, using Cytoscape (ver 3.8.0, RRID :

SCR_003032). Both networks were clustered according to Reactome FI scores. Sub-networks (Reactome FI Modules) were annotated for significantly enriched pathways from CellMap (RRID : SCR_010642), Reactome, KEGG (RRID : SCR_012773), NCI Pathway Interaction Database, Protein ANalysis THrough Evolutionary Relationships (PANTHER), and BioCarta databases (RRID : SCR_006917).

RESULTS

Molecular Profiling of Neuroblastoma Identifies Few Actionable Pathogenic Mutations but Multiple Copy Number-Altered Genes Involved in Transcriptional Regulation

Fresh tumor specimens were obtained from surgical biopsies and resections of 13 patients with neuroblastoma following informed consent. Median age was 2.65 (range: 1.45–7.80). The study population appropriately demonstrated the expected spectrum of pathological and cytogenetic risk features in neuroblastoma: 9/13 (70%) had stage 4 disease and 3/13 (23%) had MYCN amplification (**Supplementary Table S1**). Tumor specimens were subjected to genomic profiling while corresponding PDCs were subjected to phenotypic drug-response testing (**Figure 1A**).

Genomic profiling was performed using the OCCRA DNA panel. Among 130 genes interrogated for SNVs, 71 separate SNVs in 12 patients fulfilled criteria as sequence variants of IARC Class 3 and above according to American College of Medical Genetics standards (21); 27 of 71 SNVs were recurrent single nucleotide polymorphisms (SNPs) frequently encountered in our local population and excluded. Of the remaining 44 SNVs, 34 were Indels, amounting to a mean incidence of 3.1 mutations per case (**Figure 1B**). The most frequent mutations were encountered in TSC2, TP53, ARID1A and ARID1B (**Supplementary Table S2**). Among these, 11 were predicted by Sift scores to be deleterious (**Figure 1B**), and by PolyPhen scores, 5 as probably damaging and 4 as possibly damaging. TSC2 and TP53 mutations were observed in recognized hotspots (21) (**Figure 1C**). Two patients had germline splice variants of SMARCB1, though neither exhibited clinical phenotype of the associated Coffin-Siris syndrome (22) (**Figure 1C**).

To profile CNVs, normalized copy number of all 2998 probes were segmented to derive the mean copy number \log_2 ratios of 136 genes (**Supplementary Table S3**). Characteristic copy number losses in 1p [$n=4$ (31%)] and 11q [$n=5$ (38%)], and gains in 17q [$n=9$ (69%)] were observed (**Figure 2**). No CNVs were detected in 5 genes: FASLG, NF2, NRAS, SETBP1, SMARCB1. On unsupervised clustering, only MYCN clustered significantly from the copy number profiles of the other genes, with no significant clustering of other clinical covariates by mean copy number (**Supplementary Figure S1**). Of 4 patients with MYCN gain, 3 had massive amplifications (>10 copies) and 3 had 1p deletion. Both findings were separately verified on FISH. Among the genes with the highest mean copy numbers were transcription factors PPM1D, GNA13, STAT3 and STAT5B

(\log_2 ratios 0.568, 0.442, 0.228, 0.200, respectively) – all sited on chromosome 17q. Lowest copy number \log_2 ratios were seen in X chromosome genes ATRX (-0.666) and XIAP, and transcriptional regulators GATA1 (-0.678) and SH2D1A (-0.720 each).

High Throughput Screening of Neuroblastoma PDCs Reveals Drug Hits Targeting key Molecular Pathways Implicated in Neuroblastoma

Concurrently, PDCs were generated from the same 13 tumors and their recapitulation of the corresponding original tumors were validated as previously described (15) (**Supplementary Data 3**). To evaluate the *ex vivo* drug response phenotype, PDCs in log-phase growth were screened against an established 418-compound targeted inhibitor library and cytotoxicity normalized against DMSO negative controls (see **Supplementary Data 4**). The compound library was restricted to kinase inhibitors, to constrain target selectivity and limit off-target effects. Drug classes associated with the highest mean normalized cytotoxicity targeted cytoskeletal signaling, cell cycle, angiogenesis and PI3K/Akt/mTOR pathway (**Figure 3A**).

Overall, 351 (84.0%) compounds showed positive mean normalized cytotoxicity, among which 70 (16.7%) compounds had >33% cytotoxicity and were profiled as hits. To characterize the expected molecular targets, drugs were mapped to corresponding genes and signaling pathways according to drug library specifications. The commonest genes targeted by the 70 hits included mTOR [$n=17$ (24%)], Cdk [$n=8$, (11%)], FLT3 and JAK, [$n=5$ (7%), each] (**Figure 3B**). Correspondingly, among the identified drug hits were pan-CDK inhibitors flavopiridol and dinaciclib which are in early phase trials for neuroblastoma and advanced solid tumors (23–25), and mTOR ATP-competitive inhibitor INK128 (70.5% mean cytotoxicity) and PI3K inhibitor PIK-75, both with known preclinical activity against neuroblastoma (26, 27).

To determine the clinical significance of drug screen results, we correlated cytotoxicity and clinical variables using non-hierarchical unsupervised clustering, but no significant associations between PDC drug-response profiles and clinical variables were observed (**Supplementary Figure S2**) (28).

Correlation of Cytotoxicity and Copy Number Identify Mostly Novel Gene-Drug Associations

Having separately characterized the molecular aberrations of the patient tumors and the drug response profiles of their PDCs, we then sought to correlate both genomic and phenotypic readouts. Copy number and mutation calls of 131 genes and normalized cytotoxicity to 418 compounds were compared to determine significantly correlated gene-drug pairs. The z-score of Pearson correlation coefficients of 54,758 possible gene-drug combinations were normally distributed for both copy number and SNVs (**Figure 4A**). Selecting for significantly-correlated gene-drug pairs at 0.1 false discovery rate (FDR) cutoff, copy number and cytotoxicity were significantly correlated in 1278 gene-drug

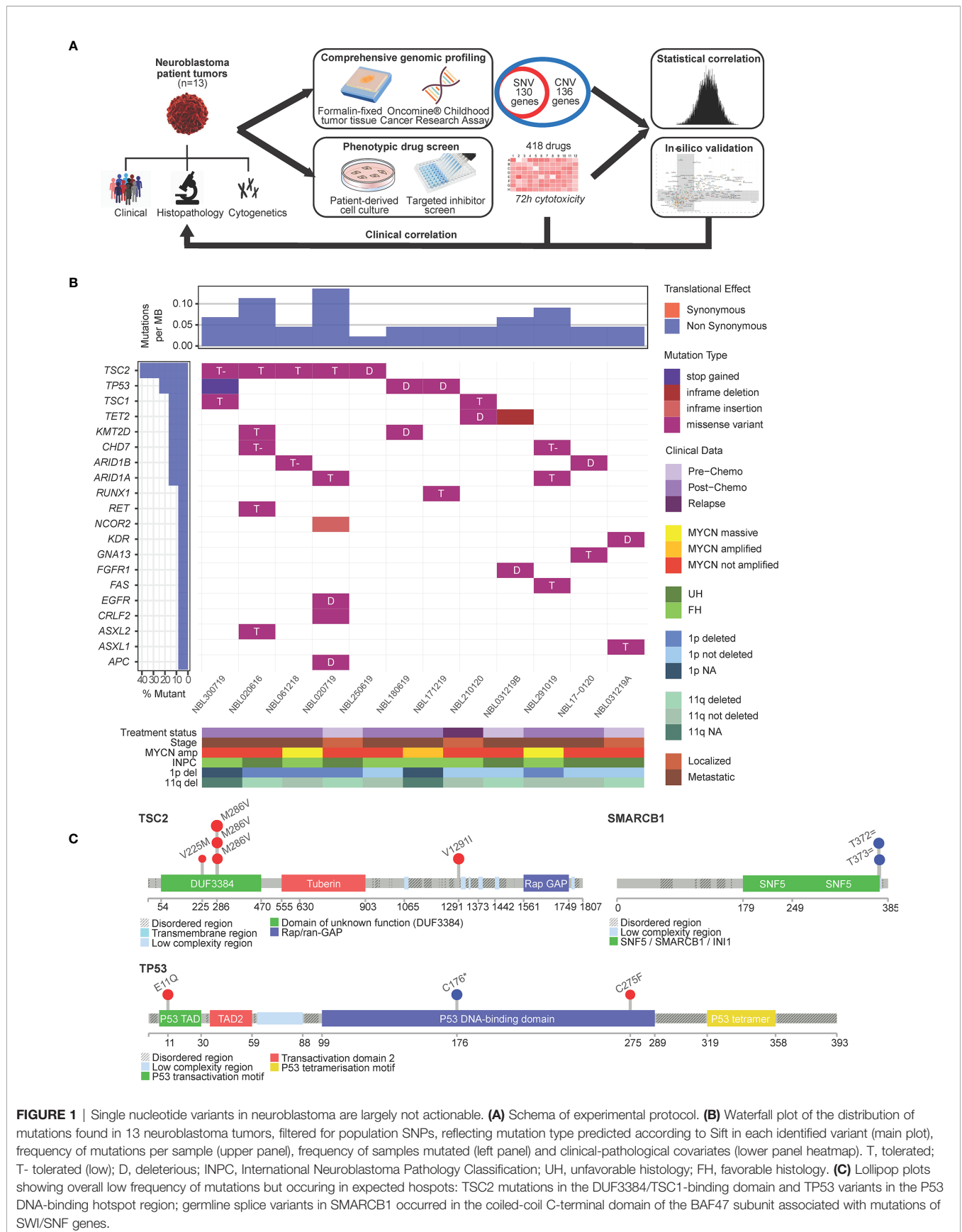


FIGURE 1 | Single nucleotide variants in neuroblastoma are largely not actionable. **(A)** Schema of experimental protocol. **(B)** Waterfall plot of the distribution of mutations found in 13 neuroblastoma tumors, filtered for population SNPs, reflecting mutation type predicted according to Sift in each identified variant (main plot), frequency of mutations per sample (upper panel), frequency of samples mutated (left panel) and clinical-pathological covariates (lower panel heatmap). T, tolerated; T- tolerated (low); D, deleterious; INPC, International Neuroblastoma Pathology Classification; UH, unfavorable histology; FH, favorable histology. **(C)** Lollipop plots showing overall low frequency of mutations but occurring in expected hotspots: TSC2 mutations in the DUF3384/TSC1-binding domain and TP53 variants in the P53 DNA-binding hotspot region; germline splice variants in SMARCB1 occurred in the coiled-coil C-terminal domain of the BAF47 subunit associated with mutations of SWI/SNF genes.

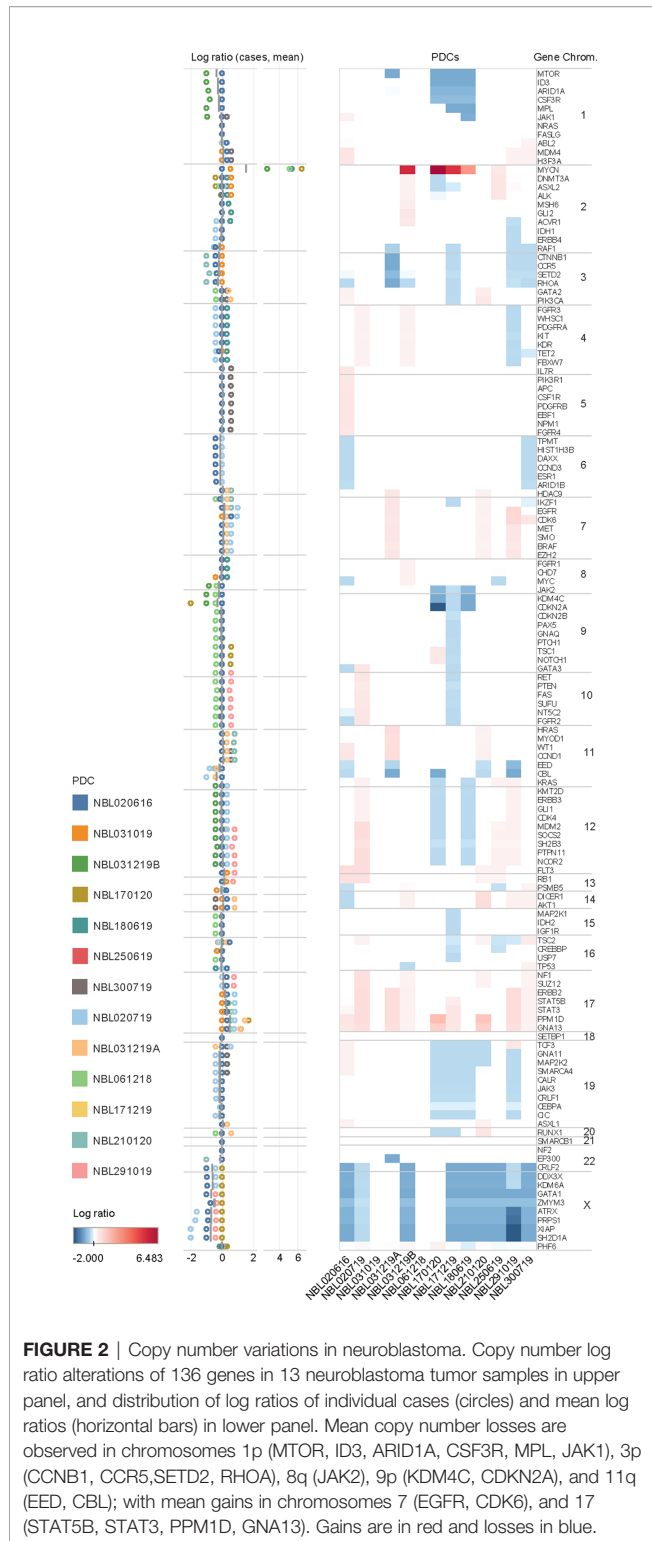


FIGURE 2 | Copy number variations in neuroblastoma. Copy number log ratio alterations of 136 genes in 13 neuroblastoma tumor samples in upper panel, and distribution of log ratios of individual cases (circles) and mean log ratios (horizontal bars) in lower panel. Mean copy number losses are observed in chromosomes 1p (MTOR, ID3, ARID1A, CSF3R, MPL, JAK1), 3p (CCNB1, CCR5, SETD2, RHOA), 8q (JAK2), 9p (KDM4C, CDKN2A), and 11q (EED, CBL); with mean gains in chromosomes 7 (EGFR, CDK6), and 17 (STAT5B, STAT3, PPM1D, GNA13). Gains are in red and losses in blue.

combinations (Supplementary Figure S3). Among these were 49 hit compounds with >33% mean cytotoxicity, which involved 159 significantly correlated gene-drug pairs (Table 1).

Due to the small number of mutations, no significant gene-drug combinations could be identified from a similar correlation

of SNVs and cytotoxicity (Figure 4A). Thus, we subsequently focused on evaluating the gene-drug pairs with significantly correlations of copy number and cytotoxicity.

To further study these observations, we compared the expected gene-drug associations (according to drug library specifications) with the significantly correlated gene-drug pairs (according to z-scores of copy number-cytotoxicity correlations) identified (Figure 4B). A total of 416 gene-drug pairs were expected (Supplementary Data 1). Among these, copy number and cytotoxicity of 4 gene-drug pairs showed significant correlations at 0.1 FDR cutoff (true positive pairs): JAK3 with AT9283, JAK1 with CYT387, FGFR1 with tyrphostin (AG1296), and FGFR3 with brivanib (BMS540215) (Figure 4C). Only the former 2 drugs demonstrated >33% cytotoxicity and qualified as hits (Figure 4C).

In 1274 gene-drug pairs, correlations were not expected but were observed. To identify pairs with the strongest treatment effect and correlation, we ranked them according to the product of their cytotoxicity and z-score (see Supplementary Data 1). Among the top- and bottom-ranked pairs, were PI3K and cell cycle agents that correlated with copy number losses of transcriptional regulators CBL and DNMT3A (log₂ ratios -0.294, and 0.039, respectively), and copy number gains of GNA13 and PPM1D (Figure 4D). The drugs most commonly associated with these pairs were PI3K/mTOR inhibitor PIK-75, and CDK inhibitors P276-00, SNS-032, AT7519, flavopiridol and dinaciclib (Supplementary Figure S4). Intertumor heterogeneity of copy-number dependent drug sensitivities were observed. For example, MYCN non-amplified tumors showed increased drug sensitivity to these agents with increased PPM1D and GNA13 copy number, while MYCN amplified tumors did not show similar trends (Supplementary Figure S4). As this was a substantial number of novel gene-drug associations that were not expected, we next verified them against available data sources and *via in-silico* modelling.

Significantly Correlated Gene-Drug Pairs Are Verified in Public Datasets

To verify if the significantly correlated gene-drug pairs were consistent with published literature, we compared them against known gene-drug associations in 6 public datasets. In each dataset, median 224 (range:46–965) pairs were identified as having an established association of drug and gene target (Supplementary Figure S5 and Supplementary Data 1). In all, 1305 of 54,758 (2.4%) pairs were identified in at least 1 dataset. Verified and unverified gene-drug pairs did not significantly differ in the distribution of cytotoxicity of the drug involved, copy number of the gene involved, and z-score of the pair across the 6 datasets (Supplementary Figure S5).

Among the 1278 significantly correlated gene-drug pairs, 19 pairs (1.5%) were verified in at least 1 data set (Supplementary Table 4) (Figure 5A), though only 1 pair (5.3%) qualified as a hit with >33% mean cytotoxicity [JAK3 with AT9283 (mean cytotoxicity 64.3 ± 16.8%)]. Among the remaining unverified 1259 gene-drug pairs, a higher percentage of pairs [12.9% (n=162)] were predicted to be hits with >33% mean cytotoxicity. Among these pairs, cytotoxicity was positively

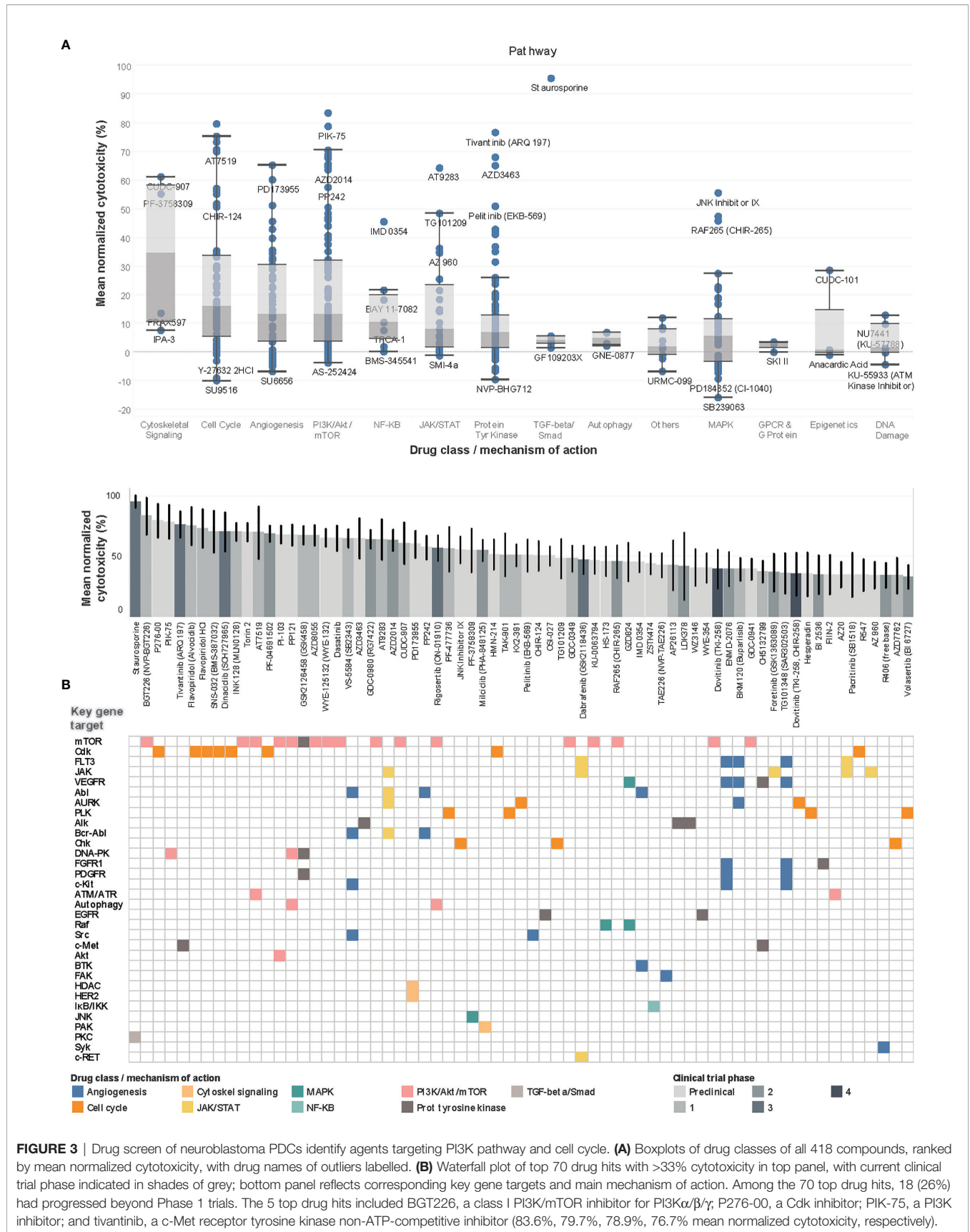


FIGURE 3 | Drug screen of neuroblastoma PDCs identify agents targeting PI3K pathway and cell cycle. **(A)** Boxplots of drug classes of all 418 compounds, ranked by mean normalized cytotoxicity, with drug names of outliers labelled. **(B)** Waterfall plot of top 70 drug hits with >33% cytotoxicity in top panel, with current clinical trial phase indicated in shades of grey; bottom panel reflects corresponding key gene targets and main mechanism of action. Among the 70 top drug hits, 18 (26%) had progressed beyond Phase 1 trials. The 5 top drug hits included BGT226, a class I PI3K/mTOR inhibitor for PI3K α / β / γ ; P276-00, a Cdk inhibitor; PIK-75, a PI3K inhibitor; and tivantinib, a c-Met receptor tyrosine kinase non-ATP-competitive inhibitor (83.6%, 79.7%, 78.9%, 76.7% mean normalized cytotoxicity, respectively).

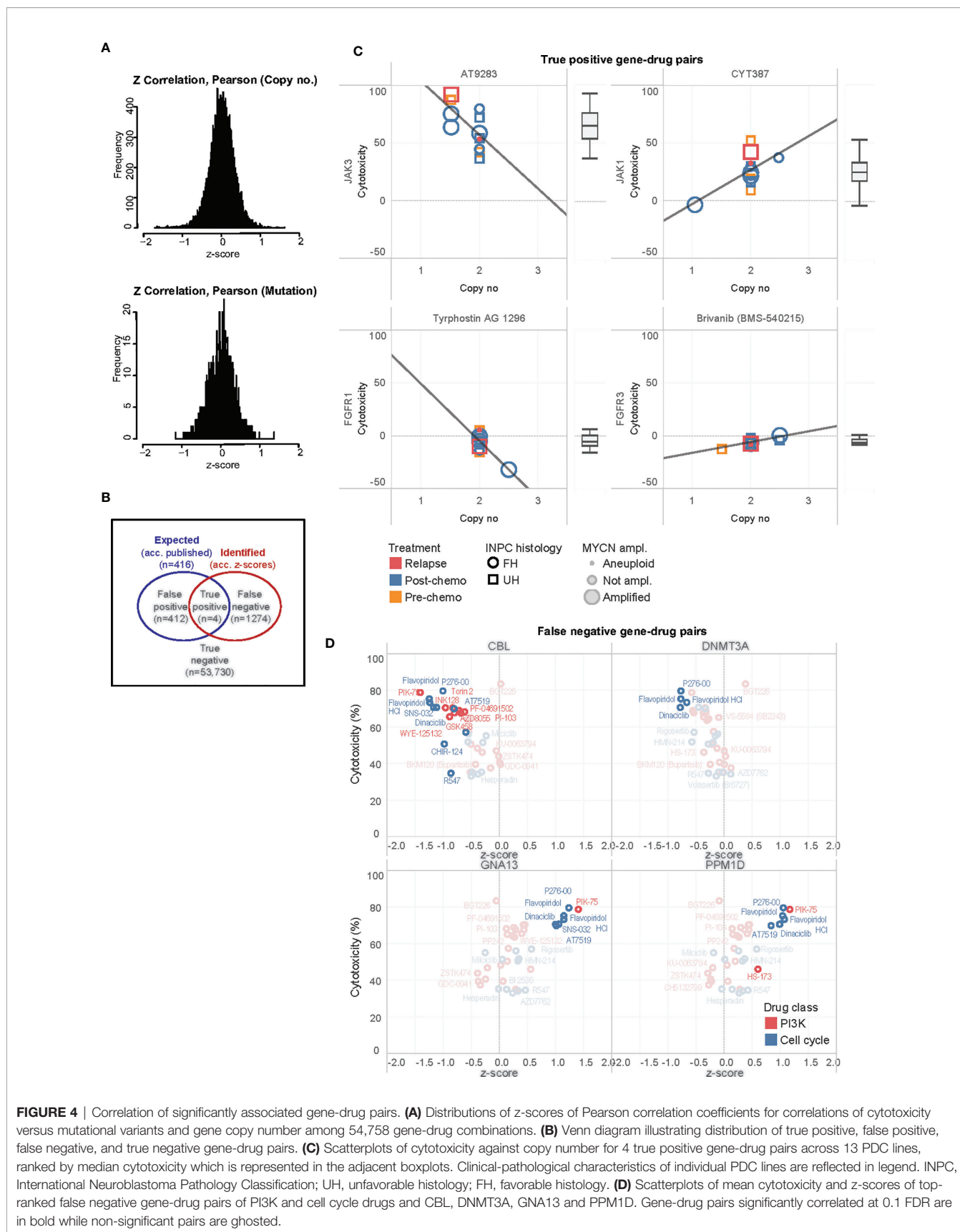


FIGURE 4 | Correlation of significantly associated gene-drug pairs. **(A)** Distributions of z-scores of Pearson correlation coefficients for correlations of cytotoxicity versus mutational variants and gene copy number among 54,758 gene-drug combinations. **(B)** Venn diagram illustrating distribution of true positive, false positive, false negative, and true negative gene-drug pairs. **(C)** Scatterplots of cytotoxicity against copy number for 4 true positive gene-drug pairs across 13 PDC lines, ranked by median cytotoxicity which is represented in the adjacent boxplots. Clinical-pathological characteristics of individual PDC lines are reflected in legend. INPC, International Neuroblastoma Pathology Classification; UH, unfavorable histology; FH, favorable histology. **(D)** Scatterplots of mean cytotoxicity and z-scores of top-ranked false negative gene-drug pairs of PI3K and cell cycle drugs and CBL, DNMT3A, GNA13 and PPM1D. Gene-drug pairs significantly correlated at 0.1 FDR are in bold while non-significant pairs are ghosted.

TABLE 1 | Pairs of drug hits and corresponding genes with significant association between cytotoxicity and copy number.

Drug	Mechanism of action	Mean cytotoxicity (S.D.)	Gene (mean copy number, z-score)
Staurosporine	TGF-beta/Smad	95.7 (± 5.5)	GNA13 (2.9, 0.73); ABL2 (2, -0.81); GNA11 (1.8, 0.86)
BGT226 (NVP-BGT226)	PI3K/Akt/mTOR	83.6 (± 16)	GNA11 (1.8, 0.86); MAP2K2 (1.8, 0.86); MPL (1.8, 0.82); JAK1 (2, 0.72)
P276-00	Cell Cycle	79.7 (± 14.5)	GNA13 (2.9, 1.23); PPM1D (3.2, 1.05); ASXL2 (2.1, -0.73); DNMT3A (2.1, -0.77); CBL (1.7, -1.01)
PIK-75	PI3K/Akt/mTOR	78.9 (± 14.5)	GNA13 (2.9, 1.4); PPM1D (3.2, 1.16); BRAF (2.2, 0.74); EZH2 (2.2, 0.74); MET (2.2, 0.74); SMO (2.2, 0.74); EED (1.8, -0.89); CBL (1.7, -1.41)
Tivantinib (ARQ 197)	Protein T.K.	76.7 (± 11.2)	GNA13 (2.9, 0.88); PPM1D (3.2, 0.75); DNMT3A (2.1, -0.72); CBL (1.7, -0.99)
Flavopiridol (Alvocidib)	Cell Cycle	75.4 (± 16.4)	GNA13 (2.9, 1.14); PPM1D (3.2, 1.04); ASXL2 (2.1, -0.71); DNMT3A (2.1, -0.77); EED (1.8, -0.79); CBL (1.7, -1.25)
Flavopiridol HCl	Cell Cycle	73.4 (± 16.7)	GNA13 (2.9, 1.14); PPM1D (3.2, 1.07); EED (1.8, -0.77); CBL (1.7, -1.24)
SNS-032 (BMS-387032)	Cell Cycle	70.8 (± 18)	GNA13 (2.9, 1.05); PPM1D (3.2, 0.98); EED (1.8, -0.75); CBL (1.7, -1.17)
Dinaciclib (SCH727965)	Cell Cycle	70.7 (± 16.9)	GNA13 (2.9, 1); PPM1D (3.2, 0.98); ASXL2 (2.1, -0.7); DNMT3A (2.1, -0.79); CBL (1.7, -1.12)
INK 128 (MLN0128)	PI3K/Akt/mTOR	70.5 (± 7.6)	CBL (1.7, -0.96)
Torin 2	PI3K/Akt/mTOR	70.4 (± 7.8)	JAK1 (2, 0.78); CBL (1.7, -0.83)
AT7519	Cell Cycle	70 (± 22.5)	GNA13 (2.9, 1.01); JAK1 (2, 0.89); PPM1D (3.2, 0.83); CBL (1.7, -0.81)
PF-04691502	PI3K/Akt/mTOR	69 (± 7.2)	CBL (1.7, -0.72)
GSK2126458 (GSK458)	PI3K/Akt/mTOR	67.8 (± 8)	NF1 (2.2, -0.7); SUZ12 (2.2, -0.7); CBL (1.7, -0.8)
AZD8055	PI3K/Akt/mTOR	67.7 (± 8.9)	JAK1 (2, 0.77)
WYE-125132 (WYE-132)	PI3K/Akt/mTOR	65.6 (± 7.7)	H3F3A (2.2, 0.75); MDM4 (2.2, 0.75); CBL (1.7, -0.89)
VS-5584 (SB2343)	PI3K/Akt/mTOR	65.2 (± 7.9)	JAK1 (2, 0.77); MPL (1.8, 0.72)
AZD3463	Protein T.K.	65.2 (± 17.4)	TCF3 (2, 0.88); JAK1 (2, 0.7)
GDC-0980 (RG7422)	PI3K/Akt/mTOR	64.5 (± 8.1)	JAK1 (2, 0.8); MPL (1.8, 0.71); TCF3 (2, 0.69)
AT9283	JAK/STAT	64.3 (± 17.4)	DNMT3A (2.1, -0.7); CBL (1.7, -0.72); CALR (1.8, -0.72); CEBPA (1.9, -0.72); CIC (1.8, -0.72); CRLF1 (1.9, -0.72); JAK3 (1.9, -0.72)
AZD2014	PI3K/Akt/mTOR	63.7 (± 9.1)	JAK1 (2, 0.87); MPL (1.8, 0.77)
PP242	PI3K/Akt/mTOR	57.6 (± 10.3)	TCF3 (2, 0.76); MPL (1.8, 0.75); JAK1 (2, 0.73)
Rigosertib (ON-01910)	Cell Cycle	57.2 (± 10.9)	JAK1 (2, 0.89); PHF6 (2.1, 0.71)
PF-477736	Cell Cycle	56.2 (± 19.2)	JAK1 (2, 1)
JNK Inhibitor IX	MAPK	55.6 (± 11.4)	JAK1 (2, 0.85)
PF-3758309	Cytoskeletal Signaling	55.2 (± 18.7)	JAK1 (2, 0.85); CBL (1.7, -0.94)
Miliciclib (PHA-848125)	Cell Cycle	55.2 (± 9.1)	ASXL1 (2.1, -0.7)
HMN-214	Cell Cycle	51.9 (± 13)	JAK1 (2, 0.72)
TAK-901	Cell Cycle	51.6 (± 18.3)	JAK1 (2, 0.85)
KX2-391	Angiogenesis	51.2 (± 9.4)	JAK1 (2, 0.76); GNA13 (2.9, 0.71); ASXL2 (2.1, -0.74); DNMT3A (2.1, -0.75)
Pelitinib (EKB-569)	Protein T.K.	51 (± 13.7)	RUNX1 (2, -0.73)
CHIR-124	Cell Cycle	50.7 (± 12.7)	FBXW7 (2, -0.73); FGFR3 (2, -0.73); KDR (2, -0.73); KIT (2, -0.73); PDGFRA (2, -0.73); CBL (1.7, -0.98)
OSI-027	PI3K/Akt/mTOR	50.5 (± 8.1)	CRLF2 (1.4, 0.89); DDX3X (1.4, 0.89); KDM6A (1.4, 0.89); MPL (1.8, 0.77); ABL1 (2, 0.71); NOTCH1 (2, 0.71)
TG101209	JAK/STAT	48.5 (± 16.8)	TCF3 (2, 0.89)
GDC-0349	PI3K/Akt/mTOR	48.4 (± 11.1)	JAK1 (2, 0.72); TCF3 (2, 0.7)
KU-0063794	PI3K/Akt/mTOR	47 (± 11.5)	GNA11 (1.8, 0.85); MAP2K2 (1.8, 0.85)
HS-173	PI3K/Akt/mTOR	46.2 (± 12.6)	PHF6 (2.1, 0.76); MYCN (27.9, 0.7)
IMD 0354	NF-KB	45.6 (± 8.5)	GNA11 (1.8, 0.85); MAP2K2 (1.8, 0.85); PHF6 (2.1, 0.76); MYCN (27.9, 0.7); PPM1D (3.2, 0.72); SMARCA4 (1.9, -0.73); GNA11 (1.8, -0.84); MAP2K2 (1.8, -0.84); APC (2.1, -0.89); CSF1R (2.1, -0.89); EBF1 (2.1, -0.89); FGFR4 (2.1, -0.89); IL7R (2.1, -0.89)
AP26113	Protein T.K.	42.9 (± 21.3)	H3F3A (2.2, 0.89); MDM4 (2.2, 0.89); TCF3 (2, 0.78); JAK1 (2, 0.74); ARID1B (1.9, -0.7); CCND3 (1.9, -0.7); DAXX (1.9, -0.7); ESR1 (1.9, -0.7); HIST1H3B (1.9, -0.7)
LDK378	Protein T.K.	42.1 (± 28.8)	H3F3A (2.2, 0.95); MDM4 (2.2, 0.95); TCF3 (2, 0.91); GNA11 (1.8, 0.79); MAP2K2 (1.8, 0.79); ARID1B (1.9, -0.82); CCND3 (1.9, -0.82); DAXX (1.9, -0.82); ESR1 (1.9, -0.82); HIST1H3B (1.9, -0.82)

(Continued)

TABLE 1 | Continued

Drug	Mechanism of action	Mean cytotoxicity (S.D.)	Gene (mean copy number, z-score)
TG101348 (SAR302503)	JAK/STAT	36.3 (± 17.3)	TCF3 (2, 0.9); H3F3A (2.2, 0.71); MDM4 (2.2, 0.71); GNA11 (1.8, 0.7); MAP2K2 (1.8, 0.7)
BI 2536	Cell Cycle	35.2 (± 16.6)	H3F3A (2.2, 0.82); MDM4 (2.2, 0.82)
FIIN-2	Protein T.K.	35.2 (± 17)	JAK1 (2, 0.75)
AZ20	PI3K/Akt/mTOR	35.2 (± 11)	JAK1 (2, 0.88)
Pacritinib (SB1518)	JAK/STAT	35.1 (± 19.1)	H3F3A (2.2, 0.88); MDM4 (2.2, 0.88); TCF3 (2, 0.78); CBL (1.7, -0.72)
R547	Cell Cycle	34.8 (± 13.7)	CBL (1.7, -0.87)
R406 (free base)	Angiogenesis	34.6 (± 10.8)	AKT1 (2.2, -0.8); DICER1 (2.2, -0.8); ASXL1 (2.1, -0.83); PIK3CA (2.1, -0.9); RUNX1 (2, -1.05)
AZD7762	Cell Cycle	34.3 (± 15.3)	JAK1 (2, 0.89)
Volasertib (BI 6727)	Cell Cycle	33.2 (± 10.1)	H3F3A (2.2, 0.79); MDM4 (2.2, 0.79); MPL (1.8, 0.7)

T.K., tyrosine kinase.

associated with copy number of GNA13, PPM1D, JAK1, and MAP2K2, and inversely associated with copy number of CBL, EED, DNMT3A and ASXL2. The drugs most commonly associated with these pairs were PI3K inhibitors PIK-75 and P276-00, and CDK inhibitors SNS-032, flavopiridol and dinaciclib (**Supplementary Tables 5, 6**) – similar to the commonest genes and drugs identified from the above comparison with specified targets of the drug library. The high incidence of hits among unverified top gene-drug pairs further suggested that important gene-drug relationships may exist among this group, and warranted further exploration.

Identified Gene-Drug Associations Are Replicated in Probabilistic *In-Silico* Model and Reveal Gene-Drug Subnetworks Centered Around PI3K and JAK-STAT Signaling

Since published data on this majority of the significantly correlated gene-drug relationships was lacking, we performed an *in-silico* prediction of how the CNV profile of our neuroblastoma tumors would be expected to influence drug response, and compared that with the corresponding z-score-based relationships. We constructed a Probabilistic Graphical Model (PGM) network by weighting our CNV data with Reactome pathway-based interactions to infer variations in inter-gene relationships (17, 19), then overlaying networks with associated Cancer Targetome drugs (20) (**Figure 5B**). A corresponding network was constructed from the 1278 significantly correlated gene-drug pairs and weighted according to z-scores (**Figure 5C**). Both networks were clustered according to Reactome Functional Interaction (FI) scores, and sub-networks of commonly represented drugs were examined.

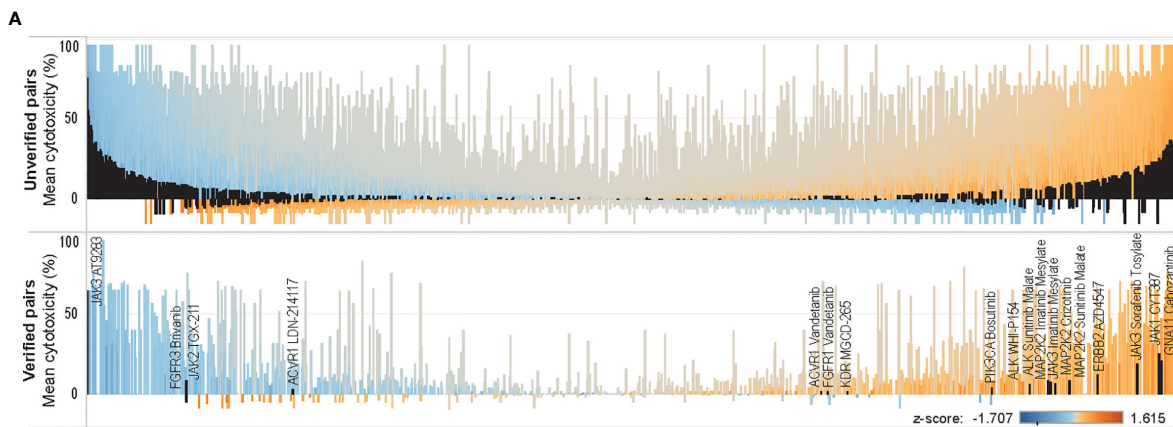
Since the curated source included only FDA-approved cancer drugs, as expected only verified gene-drug pairs were found in the PGM network (**Supplementary Data 1**). Among them, gene-drug pairs involving sunitinib and vandetanib were modeled by the PGM network – both receptor tyrosine kinase inhibitors with known effects against neuroblastoma (29–31). Examples in **Figure 5D** show how the PGM, derived only from CNV data,

predicted associations between sunitinib malate and ALK and MAP2K2, and between vandetanib and ACVR1 and FGFR1 – which were similarly demonstrated in the z-score-weighted network. The similarities observed between the CNV-based PGM predictions and the z-score-weighted network supported the integrity of the gene-drug associations identified by our experimental system.

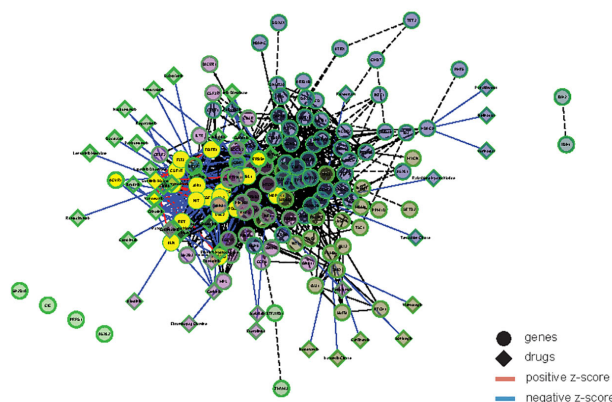
Since FI-based clustering might reveal associations between drugs and signaling pathways with potential functional significance, we isolated FI-clustered sub-networks of gene-drug pairs and annotated them for enriched Reactome pathways and Gene Ontology features (**Supplementary Data 2**). Interestingly, 2 sub-networks coincided with the unverified significantly associated gene-drug pairs that were earlier identified (**Supplementary Figures S6A, B**). In the former, copy number of ALK, DNMT3A and ASXL2 was inversely associated with efficacy of multiple kinase inhibitors like saracatinib (Module 1). In the latter, copy number of 17q genes CBL, PPM1D and GNA13 were positively associated with cytotoxicity to dinaciclib, flavopiridol and ponatinib (Module 8). Other sub-networks shared common involvement of the PI3K-mTOR (Modules 3, 6, 11), JAK-STAT (Modules 0, 3, 5, 6) pathways. Notably the z-score network also illustrated the lack of inhibitors associating with MYCN despite its substantial degree of copy number amplification.

DISCUSSION

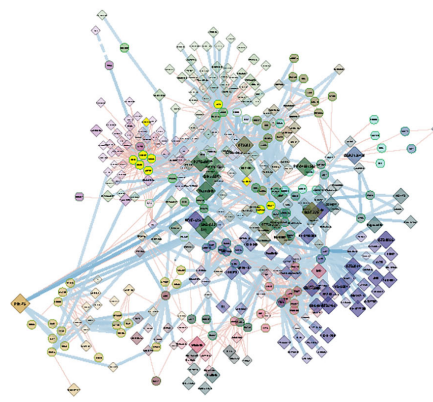
CNVs are more prevalent in mutationally quiet embryonal cancers like neuroblastoma and may reflect fundamental oncogenic dependencies that can be potentially exploited for cancer therapeutics – particularly since this phenomenon has already been utilized to target oncogene amplifications in adult cancers. In this study we hypothesized that CNVs may modulate gene dosage and correspondingly, drug response to respective targeted inhibitors. Thus, we integrated diagnostic-grade genomic profiling with phenotypic readouts of personalized preclinical tumor models to identify copy number-dependent



B Probabilistic graphical model (from CNV only)
Weighted by Reactome Functional Interaction scores



C Gene-drug network (from cytotoxicity and CNVs)
Weighted by z-scores



D

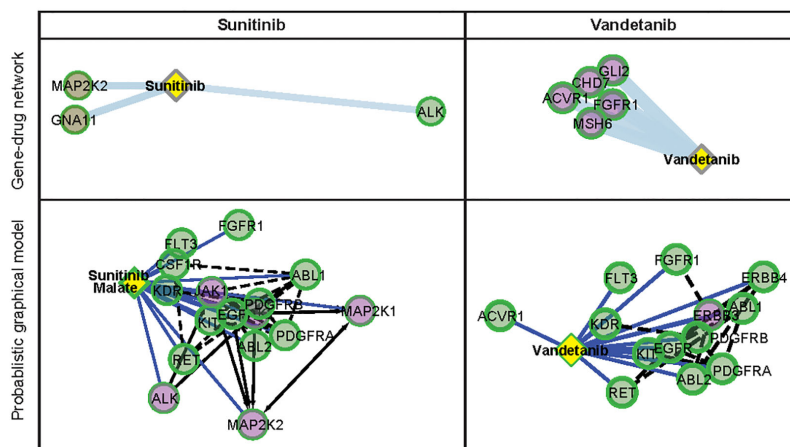


FIGURE 5 | *In-silico* validation of gene-drug pairs. **(A)** Parallel waterfall plots of the mean cytotoxicity of drugs unverified or verified in public datasets, ranked by the product of their z-scores and cytotoxicity; with similar distribution of z-scores and cytotoxicity are seen among both groups. Significantly correlated gene-drug pairs in each group are indicated in black [upper panel: 1259 of 55,543 unverified gene-drug pairs, lower panel: 19 of 1305 verified gene-drug pairs (total 54,758 gene-drug pairs)], color scale indicates z-scores. **(B)** ReactomeFIViz Probabilistic Graphical Model (PGM) constructed from weighted factors derived from CNV of 131 OCCRA genes in 13 neuroblastoma cases, annotated with 46 associated Cancer Targetome drugs and clustered according to Reactome Functional Interaction (FI) scores; solid links indicate known associations and dotted links indicate predicted association, nodes are colored according to Reactome FI clusters **(C)** z-score weighted network of 131 OCCRA genes and 418 drugs, clustered similarly according to Reactome FI scores; width of links indicates z-score and size of diamonds indicates cytotoxicity. **(D)** Association of sunitinib and vandetanib with first-degree neighbor genes, determined by z-scores, and as predicted by PGM. Both sets of gene-drug pairs are correspondingly indicated in yellow in **(B, C)**.

therapeutic susceptibilities in patients with neuroblastoma. We used correlational coefficients to quantify the strength of association between tumor copy number and cytotoxicity of PDCs in corresponding gene-drug pairs, and validated this against public data and *in silico*. The findings defined a prioritized set of targetable copy number-altered genes and their ideal corresponding inhibitors for copy-number dependent drug targeting. To provide a statistically robust context to apply these in clinical practice, we generated prediction models of the expected therapeutic response for given degrees of copy number change for each gene-drug pair. These potentially form the basic elements of a decision-making framework that could be used to inform personalized therapeutic decisions by predicting potential drug hits based on CNVs.

While the identified SNVs were known genomic aberrations in neuroblastoma (32–34), they were mostly unactionable. This underscored the limitations of targeted mutational profiling for identifying personalized treatment options for neuroblastoma and other mutationally quiet embryonal cancers (2, 35). Among the commonest variants observed in our study cohort, TP53 mutations are still largely considered untargetable (36, 37). Similarly, options for TSC2-deficient tumors are limited and largely aimed at downstream mTOR pathway targets (38). Frequency of these SNVs differed from Western series where ALK, TERT, PTPN11 and NRAS mutations are more frequent, likely reflecting known inter-ethnic differences in mutational incidence. For example, *de novo* somatic TP53 mutations are uncommon in Western series of neuroblastoma (33), but polymorphisms such as R72P R337H are more frequent in non-Caucasian populations and are associated with varying incidence of neuroblastoma (39, 40). Similarly, recurrent mutations in TSC, ARID1A and ARID1B have been reported at a lower incidence (1.7%, 11% and 6.9%, respectively) in Western populations (41–43).

Conversely, CNVs were more prevalent and importantly, demonstrated significant and biologically consistent correlations with cytotoxicity to corresponding targeted inhibitors. PPM1D, GNA13, and STAT family genes – all on 17q and implicated in up to 70% of neuroblastomas – showed the strongest correlations of copy number and cytotoxicity to targeted inhibitors (44–50). This could be due to SCAs, which are frequent and associated with worse outcome in neuroblastoma (4, 51), and regulate sensitivity to drug response in various cancers (52–54). Hence, with the known prevalence of SCAs in neuroblastoma, these associations between CNVs of key transcription factors and sensitivity to corresponding inhibitors suggests that differential copy number may be a potential quantitative predictor of drug response in neuroblastoma.

Significant associations between PI3K/Akt/mTOR pathway genes and their corresponding inhibitors were most frequently observed, accounting for half of the top 20 drug hits. PI3K/Akt/mTOR pathway upregulation, with cytoplasmic phosphorylated Akt, occurs in 62% of neuroblastomas and is a promising therapeutic target (55, 56), due to the central role played by PI3K activation in stabilizing MYCN, rendering neuroblastoma

tumors sensitive to PI3K inhibition *via* downregulation of MYCN and corresponding tumor proliferation (27, 57). BGT226 was the most potent PI3K inhibitor identified (83.6% cytotoxicity), but its effects on neuroblastoma remain understudied, and development has been discontinued following phase I/II trials in advanced adult solid tumors for lack of efficacy, inconsistent target inhibition and dose-limiting toxicities (58, 59). PI3K α inhibitor PIK-75 (78.9% cytotoxicity) stimulates anti-neuroblastoma activity by destabilizing MYCN and sensitizing tumor cells to anthracyclines (27, 60), and indeed increased cytotoxicity with PIK-75 was associated with PPM1D and GNA13 gain, and DNMT3A, CBL, EED and ASXL2 loss. Next most potent was PI-103 (68.3% cytotoxicity), which sensitizes neuroblastoma cells to TRAIL-induced apoptosis (61), and primes them to cytotoxicity from anthracyclines (62).

Cyclin dependent kinases (CDKs) critically affect cell growth, proliferation and transcriptional regulation in neuroblastoma (63). Pan-CDK inhibitors flavopiridol and dinaciclib – both among our top hits – are in now early phase trials for neuroblastoma and advanced solid tumors (23–25). AT7519, a CDK2 inhibitor (70.0% cytotoxicity), has shown excellent preclinical anti-tumor responses against MYCN-amplified neuroblastoma (64), and is currently in phase II clinical trials for adults (NCT00390117) and children (NCT01627054). CDK4/6 expression is upregulated in 30% of neuroblastomas resulting in E2F overexpression and S and G2/M phase progression (32), and is another attractive therapeutic target. Palbociclib, a CDK4/6 inhibitor, is currently approved for advanced breast cancer and in phase III clinical trials (65); P276-00, a selective CDK4 inhibitor (79.7% cytotoxicity), has shown anti-proliferative effects against other cancers (66), but too has not been assessed in neuroblastoma.

Mixed patterns of gene-drug associations were observed in JAK/STAT pathway genes, MAPK and ALK. JAK3 showed significant correlation with its corresponding inhibitor AT9283 and qualified as a drug hit, but not with other JAK inhibitors like ruxotinib. While RAS-MAPK mutations are frequent in relapsed neuroblastoma, response to MAPK inhibitors (67), and BET and MEK inhibitors (68), have been inconsistent *in vivo*, possibly due to more complex relationships between receptor tyrosine kinase inhibitors and MAPK family genes. Similarly, we also did not find significant correlation between ALK copy number and cytotoxicity with crizotinib, but instead observed associations between ALK copy number and response to other kinase inhibitors. Despite the well-established prognostic significance of ALK mutations in neuroblastoma (69), a phase I/II clinical trial for pediatric patients with relapsed and refractory solid tumors yielded complete responses in only 1 out of 11 patients with known ALK mutations (NCT00939770) (70). Results are awaited from more recent trials for patients with ALK mutations investigating loratinib, a third generation ALK inhibitor (NCT03107988), ceritinib and ribociclib (NCT02780128), and ensartinib (NCT03155620). These findings may indicate variations in gene dosage-related sensitivity to response within drug classes.

This study was limited by the small number of cases, which may limit the robustness of the gene-drug correlations identified, and the inherent inability to test every drug hit in individual

patients. Few of our shortlisted gene-drug associations could ultimately be verified against available datasets, limiting the confidence of our observations. However, our low incidence of verified gene-drug pairs is mirrored in the other drug repurposing studies mapping gene-drug associations in human disease (71). In future, corroboration of our findings in larger cohorts, and further functional validation will be required to verify the true clinical efficacy of our identified gene-drug pairs.

Associations between gene copy number and drug response could have been influenced by prior systemic treatment, or activation of alternate signaling pathways, though these are frequently encountered in relapse clinical cases where personalized therapeutic solutions are most often pursued. For example, the higher frequency of TSC2 mutants in our series could have contributed to the high rates of sensitivity of the PDCs to PI3K/mTOR-targeted agents (72). The frequently observed massive amplifications of MYCN may have also affected responses to cell cycle agents. While MYCN is similarly recognized as an undruggable target due to the lack of appropriate drug binding surfaces on its DNA binding domain, BH3 mimetics and pan-BCL-2 inhibitors can exploit the Bcl-2 over-expression frequently accompanying MYCN amplification (73–75). Alternative treatment strategies have also been suggested that capitalize on its interactions with ALK and AURKA (76, 77).

Treatment susceptibility prediction *via* genomic profiling and phenotypic assays also have their respective limitations: genomic profiling makes fundamental assumptions on correlations between genotype and phenotypic response to targeted inhibitors, while *in vitro* models may not fully recapitulate the original tumor drug-response phenotype. Also, while OCCRA offers a more efficient and focused means to survey for meaningful genomic aberrations, other novel gene targets may be missed. Future studies could complement mutational profiling with gene expression results. Also, in future, drug sensitivity could be evaluated more accurately with three-dimensional organoid models, which may better represent the true tumor microenvironment and expression profile that may influence response to test agents (41, 78).

In conclusion, integration of individualized genomic profiling and drug screening of patient-derived models of neuroblastoma showed that susceptibility to PI3K and cell cycle agents was significantly associated with copy number gains of PI3K and STAT family genes, particularly on 17q. This approach can facilitate CNV-based quantitative treatment response prediction in other mutationally quiet embryonal cancers like neuroblastoma.

DATA AVAILABILITY STATEMENT

The original contributions presented in the study are included in the article/**Supplementary Material**. Further inquiries can be directed to the corresponding author.

ETHICS STATEMENT

The studies involving human participants were reviewed and approved by SingHealth Duke NUS Central Institutional Review

Board (number 2014/2079). Written informed consent to participate in this study was provided by the participants' legal guardian/next of kin.

AUTHOR CONTRIBUTIONS

RW: Conceptualization, Data curation, Funding acquisition, Investigation, Visualization, and Writing - original draft. MRW: Conceptualization, Data curation, Investigation, and Methodology. CK: Data curation, Investigation, and Software. SES: Formal analysis and Software. MKW: Data curation and Investigation. ST: Data curation and Project administration. KM: Data curation and Resources. KC: Data curation and Resources. MT: Investigation and Methodology. GP: Methodology and Resources. ZC: Writing - review & editing. PI: Writing - review & editing. ET: Writing - review & editing. SYS: Writing - review & editing. NGI: Supervision. QF: Conceptualization, Formal analysis, Validation. AL: Conceptualization, Funding acquisition, Formal analysis, Validation, Visualization, Supervision. All authors contributed to the article and approved the submitted version.

FUNDING

This work was supported by the VIVA Foundation for Children with Cancer (VIVA-KKH Paediatric Brain and Solid Tumour Programme), Duke NUS Medical School (grant AM-ETHOS01-19-A19); SingHealth Duke NUS Surgery Academic Clinical Programme (grant GRSG14AL). The funders had no role in study design, data collection and analysis, decision to publish, or preparation of the manuscript.

ACKNOWLEDGMENTS

The authors thank Ms Jessica HX Lim, Singapore Childhood Cancer Registry; Ms Candy SC Choo, Department of Paediatric Surgery; and Ms Eileen HQ Ng, Department of Pathology and Laboratory Medicine, KK Women's and Children's Hospital.

SUPPLEMENTARY MATERIAL

The Supplementary Material for this article can be found online at: <https://www.frontiersin.org/articles/10.3389/fonc.2021.709525/full#supplementary-material>

Supplementary Figure S1 | Unsupervised hierarchical clustering of normalized cytotoxicity of 418 drugs against 13 PDCs. Rows represent cytotoxicity (blue-red scale) and columns represent cases. INPC, International Neuroblastoma Pathology Classification; FH, favorable histology; UH, unfavorable histology; INSS, International Neuroblastoma Staging System; MOA, mechanism of action.

Supplementary Figure S2 | Unsupervised hierarchical clustering of copy number profiles of 13 neuroblastoma tumor samples. Rows represent gains (red) and losses (blue) of each gene and columns represent cases. Four tumors with

MYCN amplification clustered together, of which 3 cases had concurrent copy number losses in 1p genes MPL, CSF3R, ARID1A, and ID3, and 19p genes MAP2K2, GNA11, CIC, CALR, JAK3, CRLF1, and SMARCA4 (NBL170120, NBL061218, NBL031219B) (solid box) and 1 case had multiple losses involving chromosome 9, 10, 15 and 16p genes (NBL061218) (dotted box).

Supplementary Figure S3 | Heatmap of z-scores of 418 drugs (columns) and 136 genes (rows) using unsupervised Euclidean clustering. Blue-red color scale highlights gene-drug pairs with 2.5% top- and bottom-most z-scores. Significant clusters of genes and drugs are annotated, and corresponding OCCRA panels for respective genes are indicated in grey and black on the right panel.

Supplementary Figure S4 | Scatterplots of cytotoxicity against copy number for top 6 false negative gene-drug pairs, ranked left to right by product of cytotoxicity (%) and z-score. Clinical-pathological characteristics of individual PDC lines are reflected in legend. INPC, International Neuroblastoma Pathology Classification; UH, unfavorable histology; FH, favorable histology.

Supplementary Figure S5 | Boxplots showing distribution (median, quartiles, range) of: (top panel) copy number of matched genes, (middle panel) cytotoxicity of matched drugs, and (lower panel) z-scores of matched gene-drug pairs, verified in 6 datasets of gene-drug associations.

Supplementary Figure S6 | (A–M) z-score-weighted sub-networks determined by FI-based clustering; corresponding top 5 signaling pathways most enriched in the sub-networks are listed. Source of pathways are annotated as follows: (C) CellMap, (R) Reactome, (K) KEGG, (N) NCI PID, (P) Panther, (B) BioCarta.

Supplementary Data Sheet 1 | Genomic profiling, drug screening and Pearson correlation data.

Supplementary Data Sheet 2 | Reactome and GO annotations.

Supplementary Data Sheet 3 | Neuroblastoma PDC and tumor STR profiles.

Supplementary Data Sheet 4 | Neuroblastoma PDC growth curves.

REFERENCES

- Fletcher JI, Ziegler DS, Trahair TN, Marshall GM, Haber M, Norris MD. Too Many Targets, Not Enough Patients: Rethinking Neuroblastoma Clinical Trials. *Nat Rev Cancer* 06 (2018) 18(6):389–400. doi: 10.1038/s41568-018-0003-x
- Gröbner SN, Worst BC, Weischenfeldt J, Buchhalter I, Kleinheinz K, Rudneva VA, et al. The Landscape of Genomic Alterations Across Childhood Cancers. *Nature* (2018) 555(7696):321–7. doi: 10.1038/nature25480
- Pinto N, Mayfield JR, Raca G, Applebaum MA, Chlenski A, Sukhanova M, et al. Segmental Chromosomal Aberrations in Localized Neuroblastoma Can be Detected in Formalin-Fixed Paraffin-Embedded Tissue Samples and Are Associated With Recurrence. *Pediatr Blood Cancer* (2016) 63(6):1019–23. doi: 10.1002/pbc.25934
- Schleiermacher G, Michon J, Ribeiro A, Pierron G, Mosseri V, Rubie H, et al. Segmental Chromosomal Alterations Lead to a Higher Risk of Relapse in Infants With MYCN-Non-Amplified Localised Unresectable/Disseminated Neuroblastoma (a SIOPEN Collaborative Study). *Br J Cancer* (2011) 105(12):1940–8. doi: 10.1038/bjc.2011.472
- Rice AM, McLysaght A. Dosage Sensitivity Is a Major Determinant of Human Copy Number Variant Pathogenicity. *Nat Commun* (2017) 8:14366. doi: 10.1038/ncomms14366
- Sayles LC, Breese MR, Koehne AL, Leung SG, Lee AG, Liu HY, et al. Genome-Informed Targeted Therapy for Osteosarcoma. *Cancer Discov* (2019) 9(1):46–63. doi: 10.1158/2159-8290.CD-17-1152
- Hiemzenz MC, Ostrow DG, Busse TM, Buckley J, Maglente DT, Bootwalla M, et al. OncoKids: A Comprehensive Next-Generation Sequencing Panel for Pediatric Malignancies. *J Mol Diagn* (2018) 20(6):765–76. doi: 10.1016/j.jmoldx.2018.06.009
- Ji J, Navid F, Hiemzenz MC, Kaneko M, Zhou S, Saitta SC, Biegel JA. Embryonal Rhabdomyosarcoma in a Patient With a Germline CBL Pathogenic Variant. *Cancer Genet* (2019) 231–232:62–6. doi: 10.1016/j.cancergen.2018.12.006
- Johnson JI, Decker S, Zaharevitz D, Rubinstein LV, Venditti JM, Schepartz S, et al. Relationships Between Drug Activity in NCI Preclinical *In Vitro* and *In Vivo* Models and Early Clinical Trials. *Br J Cancer* (2001) 84(10):1424–31. doi: 10.1054/bjoc.2001.1796
- Kerbel RS. Human Tumor Xenografts as Predictive Preclinical Models for Anticancer Drug Activity in Humans: Better Than Commonly Perceived-But They Can Be Improved. *Cancer Biol Ther* (2003) 2(4 Suppl 1):S134–9. doi: 10.4161/cbt.213
- Teicher BA. Tumor Models for Efficacy Determination. *Mol Cancer Ther* (2006) 5(10):2435–43. doi: 10.1158/1535-7163.MCT-06-0391
- Voskoglou-Nomikos T, Pater JL, Seymour L. Clinical Predictive Value of the *In Vitro* Cell Line, Human Xenograft, and Mouse Allograft Preclinical Cancer Models. *Clin Cancer Res* Sep (2003) 9(11):4227–39.
- Bibby MC. Orthotopic Models of Cancer for Preclinical Drug Evaluation: Advantages and Disadvantages. *Eur J Cancer* (2004) 40(6):852–7. doi: 10.1016/j.ejca.2003.11.021
- Sausville EA, Burger AM. Contributions of Human Tumor Xenografts to Anticancer Drug Development. *Cancer Res* (2006) 66(7):3351–4, discussion 3354. doi: 10.1158/0008-5472.CAN-05-3627
- Hee E, Wong MK, Tan SH, Choo Z, Kuick CH, Ling S, et al. Neuroblastoma Patient-Derived Cultures Are Enriched for a Mesenchymal Gene Signature and Reflect Individual Drug Response. *Cancer Sci* (2020) 111(10):3780–92. doi: 10.1111/cas.14610
- Benjamini Y, Hochberg Y. Controlling the False Discovery Rate: A Practical and Powerful Approach to Multiple Testing. *J R Stat Soc Ser B (Methodological)* (1995) 57(1):289–300. doi: 10.1111/j.2517-6161.1995.tb02031.x
- Wu G, Dawson E, Duong A, Haw R, Stein L. ReactomeFIViz: A Cytoscape App for Pathway and Network-Based Data Analysis. *F1000Res* (2014) 3:146. doi: 10.12688/f1000research.4431.2
- Blucher AS, McWeeney SK, Stein L, Wu G. Visualization of Drug Target Interactions in the Contexts of Pathways and Networks With ReactomeFIViz. *F1000Res* (2019) 8:908. doi: 10.12688/f1000research.19592.1
- Vaske CJ, Benz SC, Sanborn JZ, Earl D, Szeto C, Zhu J, et al. Inference of Patient-Specific Pathway Activities From Multi-Dimensional Cancer Genomics Data Using PARADIGM. *Bioinformatics* (2010) 26(12):i237–45. doi: 10.1093/bioinformatics/btq182
- Blucher AS, Choonoo G, Kulesz-Martin M, Wu G, McWeeney SK. Evidence-Based Precision Oncology With the Cancer Targetome. *Trends Pharmacol Sci* (2017) 38(12):1085–99. doi: 10.1016/j.tips.2017.08.006
- Martin KR, Zhou W, Bowman MJ, Shih J, Au KS, Dittenhafer-Reed KE, et al. The Genomic Landscape of Tuberosus Sclerosis Complex. *Nat Commun* (2017) 8:15816. doi: 10.1038/ncomms15816
- Valencia AM, Collings CK, Dao HT, St Pierre R, Cheng YC, Huang J, et al. Recurrent SMARCB1 Mutations Reveal a Nucleosome Acidic Patch Interaction Site That Potentiates mSWI/SNF Complex Chromatin Remodeling. *Cell* (2019) 179(6):1342–56.e23. doi: 10.1016/j.cell.2019.10.044
- Puppo M, Pastorino S, Melillo G, Pezzolo A, Varesio L, Bosco MC. Induction of Apoptosis by Flavopiridol in Human Neuroblastoma Cells Is Enhanced Under Hypoxia and Associated With N-Myc Proto-Oncogene Down-Regulation. *Clin Cancer Res* (2004) 10(24):8704–19. doi: 10.1158/1078-0432.CCR-03-0422
- Huang JM, Sheard MA, Ji L, Sposto R, Keshelava N. Combination of Vorinostat and Flavopiridol Is Selectively Cytotoxic to Multidrug-Resistant Neuroblastoma Cell Lines With Mutant TP53. *Mol Cancer Ther* (2010) 9(12):3289–301. doi: 10.1158/1535-7163.MCT-10-0562
- Chen Z, Wang Z, Pang JC, Yu Y, Bieerkehazhi S, Lu J, et al. Multiple CDK Inhibitor Dinaciclib Suppresses Neuroblastoma Growth via Inhibiting CDK2 and CDK9 Activity. *Sci Rep* (2016) 6:29090. doi: 10.1038/srep29090

26. Zhang H, Dou J, Yu Y, Zhao Y, Fan Y, Cheng J, et al. mTOR ATP-Competitive Inhibitor INK128 Inhibits Neuroblastoma Growth via Blocking mTORC Signaling. *Apoptosis* (2015) 20(1):50–62. doi: 10.1007/s10495-014-1066-0
27. Cage TA, Chanthery Y, Chesler L, Grimmer M, Knight Z, Shokat K, et al. Downregulation of MYCN Through PI3K Inhibition in Mouse Models of Pediatric Neural Cancer. *Front Oncol* (2015) 5:111. doi: 10.3389/fonc.2015.00111
28. Campbell K, Gastier-Foster JM, Mann M, Naranjo AH, Van Ryn C, Bagatell R, et al. Association of MYCN Copy Number With Clinical Features, Tumor Biology, and Outcomes in Neuroblastoma: A Report From the Children's Oncology Group. *Cancer* (2017) 123(21):4224–35. doi: 10.1002/cncr.30873
29. Li C, Yang C, Wei G. Vandetanib Inhibits Cisplatin-Resistant Neuroblastoma Tumor Growth and Invasion. *Oncol Rep* (2018) 39(4):1757–64. doi: 10.3892/or.2018.6255
30. Rössler J, Monnet Y, Farace F, Opolon P, Daudigeos-Dubus E, Bourredjem A, et al. The Selective VEGFR1-3 Inhibitor Axitinib (AG-013736) Shows Antitumor Activity in Human Neuroblastoma Xenografts. *Int J Cancer*. (2011) 128(11):2748–58. doi: 10.1002/ijc.25611
31. Calero R, Morchon E, Johnsen JI, Serrano R. Sunitinib Suppress Neuroblastoma Growth Through Degradation of MYCN and Inhibition of Angiogenesis. *PLoS One* (2014) 9(4):e95628. doi: 10.1371/journal.pone.0095628
32. Molenaar JJ, Koster J, Ebus ME, van Sluis P, Westerhout EM, de Preter K, et al. Copy Number Defects of G1-Cell Cycle Genes in Neuroblastoma Are Frequent and Correlate With High Expression of E2F Target Genes and a Poor Prognosis. *Genes Chromosomes Cancer* (2012) 51(1):10–9. doi: 10.1002/gcc.20926
33. Pugh TJ, Morozova O, Attiyeh EF, Asgharzadeh S, Wei JS, Auclair D, et al. The Genetic Landscape of High-Risk Neuroblastoma. *Nat Genet* (2013) 45(3):279–84. doi: 10.1038/ng.2529
34. Lasorsa VA, Formicola D, Pignataro P, Cimmino F, Calabrese FM, Mora J, et al. Exome and Deep Sequencing of Clinically Aggressive Neuroblastoma Reveal Somatic Mutations That Affect Key Pathways Involved in Cancer Progression. *Oncotarget* (2016) 7(16):21840–52. doi: 10.18632/oncotarget.8187
35. Downing JR, Wilson RK, Zhang J, Mardis ER, Pui CH, Ding L, et al. The Pediatric Cancer Genome Project. *Nat Genet* (2012) 44(6):619–22. doi: 10.1038/ng.2287
36. Arnold V, Schmelz K, Proba J, Winkler A, Wünschel J, Toedling J, et al. Reactivating TP53 Signaling by the Novel MDM2 Inhibitor DS-3032b as a Therapeutic Option for High-Risk Neuroblastoma. *Oncotarget* (2018) 9(2):2304–19. doi: 10.18632/oncotarget.23409
37. Slack A, Lozano G, Shohet JM. MDM2 as MYCN Transcriptional Target: Implications for Neuroblastoma Pathogenesis. *Cancer Lett* (2005) 228(1-2):21–7. doi: 10.1016/j.canlet.2005.01.050
38. Belaid A, Filippakis H, Lam H, Valvezan A, Huang R, Xia M, et al. Abstract A09: Therapeutic Targeting of TSC2-Deficient Cells With Methotrexate: Results of a Drug Repurposing Screen. *Clin Cancer Res* (2017) 23(1 Supplement):A09–9. doi: 10.1158/1557-3265.pmccavuln16-a09
39. Seidinger AL, Fortes FP, Mastellaro MJ, Cardinali IA, Zambaldi LG, Aguiar SS, et al. Occurrence of Neuroblastoma Among TP53 P.R337H Carriers. *PLoS One* (2015) 10(10):e0140356. doi: 10.1371/journal.pone.0140356
40. He J, Wang F, Zhu J, Zhang Z, Zou Y, Zhang R, et al. The TP53 Gene Rs1042522 C>G Polymorphism and Neuroblastoma Risk in Chinese Children. *Aging (Albany NY)*. (2017) 9(3):852–9. doi: 10.18632/aging.101196
41. Parsons DW, Roy A, Yang Y, Wang T, Scollon S, Bergstrom K, et al. Diagnostic Yield of Clinical Tumor and Germline Whole-Exome Sequencing for Children With Solid Tumors. *JAMA Oncol* (2016) 2(5):616–24. doi: 10.1001/jamaoncol.2015.5699
42. Lee SH, Kim JS, Zheng S, Huse JT, Bae JS, Lee JW, et al. ARID1B Alterations Identify Aggressive Tumors in Neuroblastoma. *Oncotarget* (2017) 8(28):45943–50. doi: 10.18632/oncotarget.17500
43. Sausen M, Leary RJ, Jones S, Wu J, Reynolds CP, Liu X, et al. Integrated Genomic Analyses Identify ARID1A and ARID1B Alterations in the Childhood Cancer Neuroblastoma. *Nat Genet* (2013) 45(1):12–7. doi: 10.1038/ng.2493
44. Wang XH, Wu HY, Gao J, Gao TH, Zhang SF. IGF1R Facilitates Epithelial-Mesenchymal Transition and Cancer Stem Cell Properties in Neuroblastoma via the STAT3/AKT Axis. *Cancer Manag Res* (2019) 11:5459–72. doi: 10.2147/CMAR.S196862
45. Saito-Ohara F, Imoto I, Inoue J, Hosoi H, Nakagawara A, Sugimoto T, et al. PPM1D is a Potential Target for 17q Gain in Neuroblastoma. *Cancer Res Apr* (2003) 63(8):1876–83.
46. Hackett CS, Hodgson JG, Law ME, Fridlyand J, Osoegawa K, de Jong PJ, et al. Genome-Wide Array CGH Analysis of Murine Neuroblastoma Reveals Distinct Genomic Aberrations Which Parallel Those in Human Tumors. *Cancer Res Sep* (2003) 63(17):5266–73.
47. Richter M, Dayaram T, Gilmartin AG, Ganji G, Pemmasani SK, Van Der Key H, et al. WIP1 Phosphatase as a Potential Therapeutic Target in Neuroblastoma. *PLoS One* (2015) 10(2):e0115635. doi: 10.1371/journal.pone.0115635
48. Petrov I, Suntsova M, Ilnitskaya E, Roumiantsev S, Sorokin M, Garazha A, et al. Gene Expression and Molecular Pathway Activation Signatures of MYCN-Amplified Neuroblastomas. *Oncotarget* (2017) 8(48):83768–80. doi: 10.18632/oncotarget.19662
49. Yan S, Li Z, Thiele CJ. Inhibition of STAT3 With Orally Active JAK Inhibitor, AZD1480, Decreases Tumor Growth in Neuroblastoma and Pediatric Sarcomas *In Vitro* and *In Vivo*. *Oncotarget* (2013) 4(3):433–45. doi: 10.18632/oncotarget.930
50. Yoge O, Almeida GS, Barker KT, George SL, Kwok C, Campbell J, et al. *In Vivo* Modeling of Chemoresistant Neuroblastoma Provides New Insights Into Chemorefractory Disease and Metastasis. *Cancer Res* (2019) 79(20):5382–93. doi: 10.1158/0008-5472.CAN-18-2759
51. Schleiermacher G, Mosseri V, London WB, Maris JM, Brodeur GM, Attiyeh E, et al. Segmental Chromosomal Alterations Have Prognostic Impact in Neuroblastoma: A Report From the INRG Project. *Br J Cancer* (2012) 107(8):1418–22. doi: 10.1038/bjc.2012.375
52. Li Y, Shen Y, Zhu Z, Wen H, Feng C. Comprehensive Analysis of Copy Number Variance and Sensitivity to Common Targeted Therapy in Clear Cell Renal Cell Carcinoma: *In Silico* Analysis With *In Vitro* Validation. *Cancer Med* (2020) 9(16):6020–9. doi: 10.1002/cam4.3281
53. Bussey KJ, Chin K, Lababidi S, Reimers M, Reinhold WC, Kuo WL, et al. Integrating Data on DNA Copy Number With Gene Expression Levels and Drug Sensitivities in the NCI-60 Cell Line Panel. *Mol Cancer Ther* (2006) 5(4):853–67. doi: 10.1158/1535-7163.MCT-05-0155
54. Yasui K, Mihara S, Zhao C, Okamoto H, Saito-Ohara F, Tomida A, et al. Alteration in Copy Numbers of Genes as a Mechanism for Acquired Drug Resistance. *Cancer Res* (2004) 64(4):1403–10. doi: 10.1158/0008-5472.can-3263-2
55. Opel D, Poremba C, Simon T, Debatin KM, Fulda S. Activation of Akt Predicts Poor Outcome in Neuroblastoma. *Cancer Res* (2007) 67(2):735–45. doi: 10.1158/0008-5472.CAN-06-2201
56. Johnsen JI, Segerström L, Orrego A, Elfman L, Henriksson M, Kågedal B, et al. Inhibitors of Mammalian Target of Rapamycin Downregulate MYCN Protein Expression and Inhibit Neuroblastoma Growth *In Vitro* and *In Vivo*. *Oncogene* (2008) 27(20):2910–22. doi: 10.1038/sj.onc.1210938
57. Chesler L, Schlieve C, Goldenberg DD, Kenney A, Kim G, McMillan A, et al. Inhibition of Phosphatidylinositol 3-Kinase Destabilizes Mycn Protein and Blocks Malignant Progression in Neuroblastoma. *Cancer Res* (2006) 66(16):8139–46. doi: 10.1158/0008-5472.CAN-05-2769
58. Markman B, Tabernero J, Krop I, Shapiro GI, Siu L, Chen LC, et al. Phase I Safety, Pharmacokinetic, and Pharmacodynamic Study of the Oral Phosphatidylinositol-3-Kinase and mTOR Inhibitor BGT226 in Patients With Advanced Solid Tumors. *Ann Oncol* (2012) 23(9):2399–408. doi: 10.1093/annonc/mds011
59. Minami H, Fujiwara Y, Muro K, Sato M, Moriya A. Phase I Study of BGT226, a Pan-PI3K and mTOR Inhibitor, in Japanese Patients With Advanced Solid Cancers. *Cancer Chemother Pharmacol* (2019) 84(2):337–43. doi: 10.1007/s00280-019-03883-6
60. Wojtalla A, Salm F, Christiansen DG, Cremona T, Cwiek P, Shalaby T, et al. Novel Agents Targeting the IGF-1r/PI3K Pathway Impair Cell Proliferation and Survival in Subsets of Medulloblastoma and Neuroblastoma. *PLoS One* (2012) 7(10):e47109. doi: 10.1371/journal.pone.0047109
61. Opel D, Naumann I, Schneider M, Bertele D, Debatin KM, Fulda S. Targeting Aberrant PI3K/Akt Activation by PI103 Restores Sensitivity to TRAIL-Induced Apoptosis in Neuroblastoma. *Clin Cancer Res* (2011) 17(10):3233–47. doi: 10.1158/1078-0432.CCR-10-2530

62. Bender A, Opel D, Naumann I, Kappler R, Friedman L, von Schweinitz D, et al. PI3K Inhibitors Prime Neuroblastoma Cells for Chemotherapy by Shifting the Balance Towards Pro-Apoptotic Bcl-2 Proteins and Enhanced Mitochondrial Apoptosis. *Oncogene* (2011) 30(4):494–503. doi: 10.1038/onc.2010.429
63. Stafman LL, Beierle EA. Cell Proliferation in Neuroblastoma. *Cancers (Basel)* (2016) 8(1):13. doi: 10.3390/cancers8010013
64. Dolman ME, Poon E, Ebus ME, den Hartog IJ, van Noesel CJ, Jamin Y, et al. Cyclin-Dependent Kinase Inhibitor AT7519 as a Potential Drug for MYCN-Dependent Neuroblastoma. *Clin Cancer Res* (2015) 21(22):5100–9. doi: 10.1158/1078-0432.CCR-15-0313
65. Finn RS, Crown JP, Lang I, Boer K, Bondarenko IM, Kulyk SO, et al. The Cyclin-Dependent Kinase 4/6 Inhibitor Palbociclib in Combination With Letrozole Versus Letrozole Alone as First-Line Treatment of Oestrogen Receptor-Positive, HER2-Negative, Advanced Breast Cancer (PALOMA-1/TRIO-18): A Randomised Phase 2 Study. *Lancet Oncol* (2015) 16(1):25–35. doi: 10.1016/S1470-2045(14)71159-3
66. Joshi KS, Rathos MJ, Joshi RD, Sivakumar M, Mascarenhas M, Kamble S, et al. *In Vitro* Antitumor Properties of a Novel Cyclin-Dependent Kinase Inhibitor, P276-00. *Mol Cancer Ther* (2007) 6(3):918–25. doi: 10.1158/1535-7163.MCT-06-0613
67. Eleveld TF, Oldridge DA, Bernard V, Koster J, Colmet Daage L, Diskin SJ, et al. Relapsed Neuroblastomas Show Frequent RAS-MAPK Pathway Mutations. *Nat Genet* (2015) 47(8):864–71. doi: 10.1038/ng.3333
68. Healy JR, Hart LS, Shazad AL, Gagliardi ME, Tsang M, Elias J, et al. Limited Antitumor Activity of Combined BET and MEK Inhibition in Neuroblastoma. *Pediatr Blood Cancer* (2020) 67(6):e28267. doi: 10.1002/psc.28267
69. Schleiermacher G, Javanmardi N, Bernard V, Leroy Q, Cappo J, Rio Frio T, et al. Emergence of New ALK Mutations at Relapse of Neuroblastoma. *J Clin Oncol* (2014) 32(25):2727–34. doi: 10.1200/JCO.2013.54.0674
70. Mossé YP, Lim MS, Voss SD, Wilner K, Ruffner K, Laliberte J, et al. Safety and Activity of Crizotinib for Paediatric Patients With Refractory Solid Tumours or Anaplastic Large-Cell Lymphoma: A Children's Oncology Group Phase 1 Consortium Study. *Lancet Oncol* (2013) 14(6):472–80. doi: 10.1016/S1470-2045(13)70095-0
71. Ferrero E, Agarwal P. Connecting Genetics and Gene Expression Data for Target Prioritisation and Drug Repositioning. *BioData Min* (2018) 11:7. doi: 10.1186/s13040-018-0171-y
72. Jacobs BL, McNally RM, Kim KJ, Blanco R, Privett RE, You JS, et al. Identification of Mechanically Regulated Phosphorylation Sites on Tuberlin (TSC2) That Control Mechanistic Target of Rapamycin (mTOR) Signaling. *J Biol Chem* (2017) 292(17):6987–97. doi: 10.1074/jbc.M117.777805
73. Bierbrauer A, Jacob M, Vogler M, Fulda S. A Direct Comparison of Selective BH3-Mimetics Reveals BCL-X. *Br J Cancer* (2020) 122(10):1544–51. doi: 10.1038/s41416-020-0795-9
74. Cournoyer S, Addiou A, Belounis A, Beaunoyer M, Nyalendo C, Le Gall R, et al. GX15-070 (Obatoclax), a Bcl-2 Family Proteins Inhibitor Engenders Apoptosis and Pro-Survival Autophagy and Increases Chemosensitivity in Neuroblastoma. *BMC Cancer* (2019) 19(1):1018. doi: 10.1186/s12885-019-6195-y
75. Ham J, Costa C, Sano R, Lochmann TL, Sennott EM, Patel NU, et al. Exploitation of the Apoptosis-Primed State of MYCN-Amplified Neuroblastoma to Develop a Potent and Specific Targeted Therapy Combination. *Cancer Cell* (2016) 29(2):159–72. doi: 10.1016/j.ccell.2016.01.002
76. Barone G, Anderson J, Pearson AD, Petrie K, Chesler L. New Strategies in Neuroblastoma: Therapeutic Targeting of MYCN and ALK. *Clin Cancer Res* (2013) 19(21):5814–21. doi: 10.1158/1078-0432.CCR-13-0680
77. Bayliss R, Burgess SG, Leen E, Richards MW. A Moving Target: Structure and Disorder in Pursuit of Myc Inhibitors. *Biochem Soc Trans* (2017) 45(3):709–17. doi: 10.1042/BST20160328
78. Kumar HR, Zhong X, Hoelz DJ, Rescorla FJ, Hickey RJ, Malkas LH, et al. Three-Dimensional Neuroblastoma Cell Culture: Proteomic Analysis Between Monolayer and Multicellular Tumor Spheroids. *Pediatr Surg Int* (2008) 24(11):1229–34. doi: 10.1007/s00383-008-2245-2

Conflict of Interest: The authors declare that the research was conducted in the absence of any commercial or financial relationships that could be construed as a potential conflict of interest.

Publisher's Note: All claims expressed in this article are solely those of the authors and do not necessarily represent those of their affiliated organizations, or those of the publisher, the editors and the reviewers. Any product that may be evaluated in this article, or claim that may be made by its manufacturer, is not guaranteed or endorsed by the publisher.

Copyright © 2021 Wong, Wong, Kuick, Saffari, Wong, Tan, Merchant, Chang, Thangavelu, Periyasamy, Chen, Iyer, Tan, Soh, Iyer, Fan and Loh. This is an open-access article distributed under the terms of the Creative Commons Attribution License (CC BY). The use, distribution or reproduction in other forums is permitted, provided the original author(s) and the copyright owner(s) are credited and that the original publication in this journal is cited, in accordance with accepted academic practice. No use, distribution or reproduction is permitted which does not comply with these terms.